Cellular/Molecular

Toxic Role of K^+ Channel Oxidation in Mammalian Brain

Diego Cotella,[1]* Berenice Hernandez-Enriquez,[1]* Xilong Wu,[1] Ruiqiong Li,[1] Zui Pan,[1] Joseph Leveille,[1] Christopher D. Link,[2] Salvatore Oddo,[3] and Federico Sesti[1]

[1]Department of Physiology and Biophysics, University of Medicine and Dentistry of New Jersey, Robert Wood Johnson Medical School, Piscataway, New Jersey 08854, [2]Institute for Behavioral Genetics, University of Colorado at Boulder, Boulder, Colorado 80309-0447, and [3]Department of Physiology, University of Texas Health Science Center, San Antonio, Texas 78229

Potassium (K^+) channels are essential to neuronal signaling and survival. Here we show that these proteins are targets of reactive oxygen species in mammalian brain and that their oxidation contributes to neuropathy. Thus, the KCNB1 (Kv2.1) channel, which is abundantly expressed in cortex and hippocampus, formed oligomers upon exposure to oxidizing agents. These oligomers were ~10-fold more abundant in the brain of old than young mice. Oxidant-induced oligomerization of wild-type KCNB1 enhanced apoptosis in neuronal cells subject to oxidative insults. Consequently, a KCNB1 variant resistant to oxidation, obtained by mutating a conserved cysteine to alanine, (C73A), was neuroprotective. The fact that oxidation of KCNB1 is toxic, argues that this mechanism may contribute to neuropathy in conditions characterized by high levels of oxidative stress, such as Alzheimer's disease (AD). Accordingly, oxidation of KCNB1 channels was exacerbated in the brain of a triple transgenic mouse model of AD (3xTg-AD). The C73A variant protected neuronal cells from apoptosis induced by incubation with β-amyloid peptide ($A\beta_{1-42}$). In an invertebrate model (*Caenorhabditis elegans*) that mimics aspects of AD, a C73A-KCNB1 homolog (C113S-KVS-1) protected specific neurons from apoptotic death induced by ectopic expression of human $A\beta_{1-42}$. Together, these data underscore a novel mechanism of toxicity in neurodegenerative disease.

Introduction

Potassium (K^+) channels are a diverse and ubiquitous family of ion-channels that operate in nonexcitable and excitable cells. K^+ channels are essential for the function of the nervous system where they modulate the shape and frequency of action potentials and consequently, neurotransmitter release. As such, conditions that result in the impairment of K^+ channels have the potential to cause neuronal dysfunction by affecting the excitability of the cell, which is intrinsically dependent on these proteins. For example, mutations in KCNQ2, KCNQ3, KCNMA1, KCNA1 and KCNC3 genes which lead to the synthesis of mutants with defective properties have been identified in patients affected by epilepsy, ataxia and episodic ataxia type 1 (for review, see Kullmann, 2002). In addition to genetic predisposition, acquired impairment of K^+ channel's function can lead to neurological diseases, such as, acquired neuromyotonia, limbic encephalitis, and Morvan's syndrome (for review, see Vernino, 2007).

Received Dec. 12, 2011; revised Jan. 12, 2012; accepted Feb. 3, 2012.

Author contributions: D.C., B.H.E., and F.S. designed research; D.C., B.H.E., X.W., R.L., J.L., C.D.L., and F.S. performed research; Z.P. and S.O. contributed unpublished reagents/analytic tools; D.C., B.H.E., X.W., R.L., Z.P., J.L., and C.D.L. analyzed data; F.S. wrote the paper.

This work was supported by two National Science Foundation grants (0842708 and 1026958) and an American Heart Association grant (09GRNT2250529) to FS. J.L. participated in The Research in Science and Engineering (RISE) Rutgers-UMDNJ joint program. We thank Dr. Maria Cavalletto with help with the mass-spectrometry analysis, Dr. Shiqing Cai for critical reading of the manuscript, and Dr. Shuang Liu for helpful comments on clinical aspects of AD. N2A cells were a kind gift from Dr. Mladen-Roko Masin. The KCNB1 cDNA was a gift form Dr. Steve Goldstein.

*D.C. and B.H.E. contributed equally to this work.

Correspondence should be addressed to Dr. Federico Sesti, at the above address. E-mail: sestife@umdnj.edu.

D. Cotella's present address: Dipartimento di Scienze Mediche, Laboratorio di Biologia Applicata, Universita' del Piemonte Orientale A. Avogadro, via Solaroli 17, 28100 Novara, Italy.

DOI:10.1523/JNEUROSCI.6153-11.2012

 0270-6474/12/324133-12$15.00/0

Oxygen metabolism leads to the synthesis of reactive and thus potentially toxic molecules known as reactive oxygen species (ROS). The increase in unbuffered ROS levels in a cell, a phenomenon commonly referred to as oxidative stress, is thought to cause significant cellular damage and to contribute to cellular aging (Harman, 1956). Moreover, oxidative stress is elevated in neuropathies such as Alzheimer's disease (AD) (for review, see Lin and Beal, 2006). Oxidative damage occurs early in AD, before the onset of significant plaque formation (Nunomura et al., 2001; Praticò et al., 2001; Reddy et al., 2004), and consequently, protein oxidation is extensive in AD (Hensley et al., 1995; Lauderback et al., 2001; Butterfield and Lauderback, 2002; Sultana et al., 2006). This body of evidence argues that oxidation of K^+ channels might have a role in normal aging and in neurodegenerative diseases such as AD. If modified by oxidation, KCNB1 might affect neuronal excitability and survival, thereby contributing to neurotoxicity. Initial evidence that oxidation of K^+ channels during aging is a mechanism of neurodegeneration came from an invertebrate organism, the worm *Caenorhabditis elegans*. In this animal oxidation of the voltage-gated K^+ channel, KVS-1 induced progressive alteration of neuronal excitability with consequent loss of sensory function (taste) (Cai and Sesti, 2009). Accordingly, this degeneration was stopped in transgenic worms expressing a KVS-1 mutant resistant to oxidation (C113S-KVS-1). The *C. elegans* case argues that similar mechanisms may contribute to the normal aging and neurodegeneration of the mammalian nervous system. However, the supporting evidence was, to date, limited (for review, see Sesti et al., 2010).

To address the fundamental questions of whether K^+ channels are subject to a process of oxidation during aging and whether their oxidation may contribute to neuropathy, we fo-

cused on the voltage-gated K^+ channel, KCNB1 (commonly known as Kv2.1). This channel conducts a principal component of the somatodendritic current in the pyramidal neurons of cortex and hippocampus (Misonou et al., 2005). KCNB1 has been implicated in oxidation-induced degenerative processes *in vitro* (Song, 2002; Pal et al., 2003; Misonou et al., 2005; Mankouri et al., 2009) and is the mammalian homolog of KVS-1 whose oxidation during aging is a primary cause of sensory function loss in *C. elegans* (Rojas et al., 2008; Cai and Sesti, 2009).

Here we show that KCNB1 is subject to a process of oxidation in normal and AD mouse brain and most importantly, that its oxidation contributes to neurotoxicity.

Materials and Methods

Molecular biology

For expression in mammalian cells, KCNB1 was subcloned into the pCI-neo vector (Promega) and epitope tagged by replacing the terminal stop codon with nucleotides encoding HA residues (YPYDVPDYA-STOP). Cysteine mutants were constructed by site-directed mutagenesis using *Pfu* polymerase (Stratagene) and the KCNB1-HA plasmid as template. The $A\beta_{1-42}$ construct was obtained by subcloning the human $A\beta_{1-42}$ cDNA containing the artificial signal peptide coding sequence for expression in *C. elegans* (Link, 1995) into a pPD95.75 Fire vector containing the *flp-6* promoter sequence (Cai and Sesti, 2009).

Biochemistry

To avoid unspecific oxidation, the following measures were taken: (1) dissolved molecular oxygen was removed from the lysis buffers by gurgling nitrogen into the solution: (2) 10 mM iodoacetamide was added to the lysis buffers; (3) high-speed, long centrifugation steps were avoided.

Cell cultures. CHO-K1 cells were grown in HAM-F12 medium with 10% FBS. Cells were transfected at 90% confluence using Lipofectamine 2000 (Invitrogen). Twenty-4 h after transfection, the cells were washed with PBS and chemicals were added for 5–10 min. Then, the solutions were removed and the cells were lysed in 200 μl of 4× Laemmli buffer without reducing reagents. Proteins were resolved by 8% SDS-PAGE under nonreducing conditions and transferred to a PVDF membrane. The membrane was incubated in a 5% solution of nonfat milk in Tween 20-PBS (PBST) for 2 h at room temperature. After overnight incubation at 4°C with the primary antibody the membrane was washed for 20 min and incubated at room temperature with the appropriate secondary antibody. The blot was washed in PBST for 20 min and incubated for 5 min with POD chemiluminescence substrates and exposed. Densitometry analysis was performed using ImageJ (NIH) software.

Mouse brains. Frozen, half sagittal brains of either sex were homogenized with a glass tissue grinder in lysis buffer (0.32 M sucrose, 5 mM Tris-Cl, pH 6.8, 0.5 mM EDTA, 1 mM PMSF and protease inhibitor cocktail set I (Calbiochem). Samples were centrifuged at 2000 rpm for 10 min and the supernatant used for biochemical analysis. Protein content was quantified with the Bradford colorimetric assay (Sigma).

Mass spectrometry

HEK 293 cells were used because they yield larger amounts of protein than CHO or N2A cells. HEK cells were transfected with calcium phosphate in a 10 cm Petri dishes with 10 μg of the hKv2.1-HA plasmid. Thirty-six hours following transfection cells were washed with PBS and exposed to 2 mM H_2O_2 (diluted in PBS) for 5 min. After washing with PBS, the cells were lysed with 1 ml of ice-cold RIPA buffer (50 mM Tris, pH 7.4, 150 mM NaCl, 1 mM EDTA, 1% IGEPAL CA-630, 0.5% (w/v) sodium deoxycholate, 0.1% (w/v) SDS, freshly added 10 mM iodoacetamide, phosphatase and protease inhibitors), sonicated for 5 s and centrifuged to remove cell debris. The supernatant was mixed with 30 μl of anti-HA agarose beads (Roche) and rocked at 4°C for 3 h. Beads were washed three times with ice-cold 1% RIPA buffer and then split in two aliquots. One aliquot was incubated in 50 μl of SDS sample buffer in the absence of reducing agents at ~90−95°C for 5 min and the other aliquot was incubated in the same SDS sample buffer containing 20 mM DTT at ~90−95°C for 5 min. Samples were run on a SDS-PAGE and the gel was stained with Coomassie blue. Bands were excised from the gel and gel slices corresponding to monomeric Kv2.1 and oligomeric Kv2.1 were in-gel digested with trypsin as follow: gel slices were destained (50% methanol, 5% acetic acid), shrunk with 100% acetonitrile (ACN) and dried in a SpeedVac. Rehydrated gel pieces were reduced with 10 mM DTT and alkylated with 100 mM iodoacetamide. Each sample was incubated at 37°C in 50 mM NH_4HCO_3 with 25 ng/ml trypsin (Roche) for 15 h. Peptides were extracted using 50% ACN, 1% trifluoroacetic acid (TFA) and analyzed by MALDI-TOF mass spectrometry. Peptide solution (1 μl) was vacuum-dried with 1 μl of matrix (1% w/v α-ciano-4-hydroxycinnamic acid in 50% ACN, 0.1% TFA). Spectra were obtained using a Voyager-DE Pro MALDI-TOF spectrometer (Applied Biosystems) operated in the delayed extraction and reflector mode. Internally calibrated spectra were processed via the Data Explorer software. Mascot Distiller (Matrix Science) was used to create peak lists from MS raw data. Mascot Server (Matrix Science) was used for database searching versus NCBInr. Carbamidomethylation of cysteine residues, oxidation of methionine, deamidation of asparagine and glutamine were set as possible variable modifications and trypsin was selected as protease.

Apoptosis assays

Apoptosis was assessed using annexin-V labeling. Cells positive to annexin-V were computed using a flow-cytometer analyzer or manually by counting the number of cells positive to annexin-V in 25 μm^2 areas (typically, 4–6 measurements). Manual experiments were performed blind. Thus, N2A cells were plated on 12 mm glass coverslips and cultured in DMEM supplemented with 10% fetal bovine serum and 1% sodium pyruvate. Cells were transfected at 90% confluence using Lipofectamine 2000. Twenty-four hours after transfection, the cells were washed with PBS and exposed to either oxidants or Aβ peptides as follows.

Oxidants. 2,2′-Dithiodipyridine (DTDP) (dissolved in DMEM) or H_2O_2 were added for 5 min. Then, the cells were washed with PBS 2 times and incubated for 6 h in fresh DMEM medium.

Aβ peptide. Hexafluoro-2-propanol (HFIP)-pretreated (to avoid aggregation) $A\beta_{1-42}$ peptide and the reverse (not HFIP-treated) $A\beta_{42-1}$ peptide were purchased from Anaspec. The peptides were added to the media (24 h after transfection) at a final concentration of 23 μg/ml and 0.0025% NH_4OH and incubated for 12 h. NH_4OH, which was used to solubilize the peptides was moderately proapoptotic ($7 \pm 0.1\%$ $n = 5$ experiments). The data presented in Figure 6 (see below) were scaled accordingly.

The cells were washed with PBS and incubated with annexin-V labeling buffer solution (20 μl of Annexin-V-Fluos and 20 μl of propidium iodide in 1 ml of incubation buffer provided by the kit. Propidium iodide detects necrotic cells) for 15 min according to manufacturer's instructions and mounted on a Olympus BX61 microscope equipped Nomarski optics and a digital camera. For flow-cytometric analysis cells were cultured in 24-wells plates, trypsinized, collected in a 1.5 ml of Eppendorf tube by centrifugation at 5000 rpm for 10 min at room temperature, dissolved in annexin-V labeling buffer solution and analyzed with a Beckman Coulter FC500 analyzer.

DCFH-DA fluorometry

N2A cells treated with 10 μM DTDP for 5 min, were incubated with 5 μM 2′,7′-dichlorofluorescein diacetate (DCFH-DA) for 30 min. DCFH-DA permeates the cell membrane and becomes hydrolyzed by intracellular esterases to nonfluorescent DCFH. In the presence of ROS, such as hydrogen peroxide, hydroxyl ions, and hydroperoxides, DCFH is oxidized to fluorescent dichlorofluorescein (DCF). Cells were washed twice with PBS analyzed with an Olympus BX61 microscope equipped with Nomarski optics and a digital camera. Digitally acquired pictures were subsequently analyzed with ImageJ 1.44 software (NIH). Data are expressed as percentage increases with respect to control values.

Electrophysiology

CHO cells were transfected using the Qiagen SuperFect kit which has a lower transfection efficiency than Lipofectamine but is more gentle to the cells. Data were recorded with an Axopatch 200B amplifier (Molecular Devices) a PC (Dell), and Clampex software (Molecular Devices). Data

were filtered at f_c = 1 kHz and sampled at 2.5 kHz. Bath solution contained the following (in mM): 4 KCl, 100 NaCl, 10 HEPES (pH = 7.5 with NaOH), 1.8 $CaCl_2$, and 1.0 $MgCl_2$. Pipette solution contained (in mM): 100 KCl, 10 HEPES (pH = 7.5 with KOH), 1.0 $MgCl_2$, 1.0 $CaCl_2$, 10 EGTA (pH = 7.5 with KOH). H_2O_2 or chloramine-T (CHT) was added fresh prior to the experiment from 8.3 M (H_2O_2) or 0.5 M stock in H_2O (CHT). Offset potentials due to series resistances (≤5 mV) were not compensated for, when generating current–voltage relationships. Macroscopic conductances were calculated as:

$$G(V) = \frac{I}{V - V_{rev}}, \quad (1)$$

where I is the steady-state current, V is the applied voltage, and V_{rev} is the computed Nernst potential for K^+ at the experimental concentrations used (−103 mV). Macroscopic conductances were fitted to the Boltzmann function:

$$G(V)/G_{Max} = \frac{1}{1 + e^{(V_{1/2}-V)/V_s}}, \quad (2)$$

where $V_{1/2}$ is the voltage at which $G/G_{Max} = 1/2$ and V_s is the slope factor. Single-channel activity was analyzed by pClamp 8 software (Molecular Devices).

Strains and construction of transgenic animals

The derivation and characterization of the 3xTg-AD mice has been described previously (Oddo et al., 2003). Briefly, two independent transgenes encoding human APP_{Swe} and the human tau_{P301L} (both under control of the mouse Thy1.2 regulatory element) were comicroinjected into single-cell embryos harvested from homozygous mutant $PS1_{M146V}$ knock-in (PS1-KI) mice.

C. elegans

Background strains were Bristol (N2) and *tm2034* (*kvs-1* KO; outcrossed four times). We constructed the following: FDX(ses19): N2(P_{flp-6}::$A\beta_{1-42}$)(P_{myo-2}::gfp), FDX(ses20): tm2034(P_{flp-6}::$A\beta_{1-42}$)(P_{KVS-1}::C113S-KVS-1)(P_{myo-2}::gfp), FDX(ses21): tm2034(P_{flp-6}::$A\beta_{1-42}$)(P_{KVS-1}::KVS-1)(P_{myo-2}::gfp), FDX(ses25): N2(P_{flp-6}::$A\beta_{1-42}$)(P_{gcy-5}::gfp)(rol-6), FDX-(ses26): tm2034(P_{flp-6}::$A\beta_{1-42}$)(P_{KVS-1}::C113S)(P_{gcy-5}::gfp)(rol-6), FDX-(ses27): tm2034(P_{flp-6}::$A\beta_{1-42}$)(P_{KVS-1}::KVS-1)(P_{gcy-5}::gfp)(rol-6).

The constructs were injected into the syncytial gonads of adult hermaphrodites. Transformant lines were stabilized by a mutagenesis-induced integration into a chromosome by irradiating 40 animals with γ-ray with 4000 rads for 40 min. The progeny were checked for 100% transmission of the marker and also for the presence of the transgene by PCR amplification.

*Behavioral assays (*C. elegans*)*

Age-synchronization. Nematodes were grown in standard 10 cm NGM plates + OP50 *E. coli* until a large population of gravid adults was reached (3–5 d). The animals were collected in 50 ml of Falcon tubes, washed in M9 buffer (22 mM KH_2PO_4, 22 mM NaH_2PO_4, 85 mM NaCl, 1 mM $MgSO_4$), and treated with 10 volumes of basic hypochlorite solution (0.25 M NaOH, 1% hypochlorite freshly mixed; no significant differences were observed in bleach-free preparations, obtained by isolating laid eggs with SDS/NaOH). Worms were incubated at room temperature for 10 min, then the eggs (and carcasses) collected by centrifugation at 400 × *g* for 5 min at 4°C, incubated overnight in M9 buffer and seeded on standard NMG plates.

Experiments were performed as described previously and without knowledge of the worms' genotype (Bianchi et al., 2003).

Chemotaxis assay. A chunk of agar 0.5 cm in diameter was removed from 10 cm plates and soaked in the attractant for 2 h. Lysine and biotin were used at concentrations of 0.5 M and 0.2 M, respectively. Chunks were put back in the plate overnight to allow equilibration and formation of a gradient. Approximately 20 age-synchronized worms were placed between the test spot and a control spot on the opposite side of the plate. Ten microliters of 20 mM NaN3 was placed on both spots. After 1 h, animals on the test/control spot were counted, and a chemotaxis index, C.I., was calculated as the number of animals at the test spot (N_{test}) minus the number of animals at the control spot ($N_{Cnt.}$), divided by the total number of animals (N). A positive C.I. indicates attraction:

$$\text{C.I.} = \frac{N_{Test} - N_{Cnt}}{N}. \quad (3)$$

An experiment was performed with ~100 worms per genotype distributed in 5 test plates.

To study chemotaxis during aging, experiments were started with ~600–1000 age-synchronized worms per genotype (mean life span ~ 20 d). Worms were examined every day until death and were scored as dead when they were no longer able to move even in response to prodding with a platinum pick. Each day, worms were transferred to a fresh plate containing bacteria.

Thrashing assay. Age-synchronized worms were picked in a drop of M9 buffer on an agar plate. After 2 min of recovery, thrashes were counted for 2 min. A thrash was defined as a change in the body bend at the mid-body point.

Primary embryonic cultures

Cultured cells were prepared as described before (Park et al., 2005). Briefly, gravid adult worms were lysed using 0.5 M NaOH and 1% NaOCl (no significant differences were observed in bleach-free preparations, obtained by isolating laid eggs with SDS/NaOH). Released eggs were washed three times with sterile egg buffer containing 118 mM NaCl, 48 mM KCl, 2 mM CaCl2, 2 mM MgCl2, and 25 mM HEPES (pH 7.3, 340 mOsm), and adult carcasses were separated from washed eggs by centrifugation in sterile 30% sucrose. Eggshells were removed by resuspending pelleted eggs in a sterile egg buffer containing 1 U/ml chitinase at room temperature for 1.5 h. Embryos were resuspended in L-15 cell culture medium containing 10% fetal bovine serum, 50 U/ml penicillin, and 50 μg/ml streptomycin (Sigma) and dissociated by gentle pipetting. Intact embryos, clumps of cells, and larvae were removed from the cell suspension by filtration. Dissociated cells were plated on glass coverslips previously coated with peanut lectin (0.1 mg/ml) dissolved in water.

Immunohistochemistry

For Aβ immunohistochemistry, transgenic worms were fixed and permeabilized as previously described (Link et al., 1992), except that glutaraldehyde was eliminated from the fixation step. Permeabilized worms were stained for Aβ using anti-Aβ monoclonal antibody 6E10 (Covance) at a final concentration of 5 μg/ml and Alexa Fluor 594-labeled goat-anti mouse secondary antibody (Invitrogen) at 20 μg/ml. Stained worms were imaged with a Zeiss Axiophot epifluorescence microscope equipped with digital deconvolution capacity (Intelligent Imaging Innovations).

Statistical analysis

Quantitative data are presented as mean ± SEM. The level of significance was calculated using Student's *t* test for single comparisons and ANOVA for multiple comparisons. Normality was assessed by the *F* test and corrections performed using a Tukey means comparison test with 95% confidence level using OriginPro 7.5 software. Statistical significance was assumed at the 95% confidence limit or greater ($p < 0.05$).

Results

The KCNB1 channel is susceptible to redox

KCNB1 channels, HA epitope tagged in the C terminus and expressed in CHO cells, run as monomers with a molecular mass ~110 kDa (Fig. 1*A*) in SDS-PAGE in the absence of denaturants in the sample buffer (native gel) or in the presence of the reducing agent DTT. Mild treatment with oxidizing agents, hydrogen peroxide (H_2O_2)or CHT led to the formation of oligomers running with molecular masses ranging from ~ 250 kDa to ~400 kDa, which were reduced upon subsequent exposure to DTT (Fig. 1*A*). Oligomer formation might be the consequence of cross-linking of channel subunits to each other or to other unknown proteins. However, no unknown proteins could be detected in Coomassie staining of immunoprecipitates of oxidized KCNB1

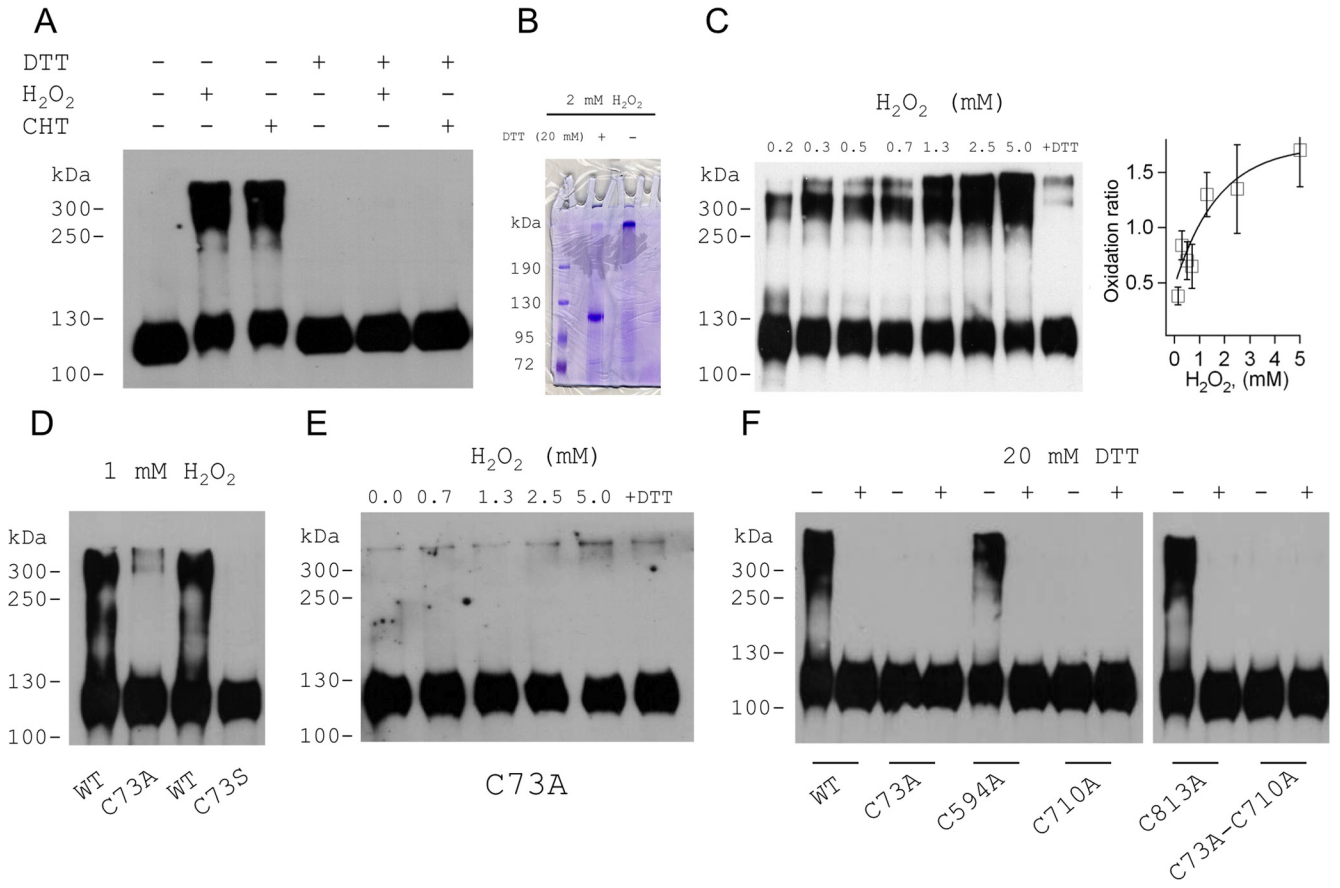

Figure 1. KCNB1 is susceptible to redox. ***A***, Western visualization (nondenaturing gel) of wild-type KCNB1-HA channels transiently expressed in CHO cells in the absence or presence of 1.0 mM H_2O_2 or CHT or 20 mM DTT (lanes 1–4). The oxidants were added for 5–10 min before lysis. In lanes 5 and 6, oxidized samples were run in reducing conditions (20 mM DTT in sample buffer). ***B***, Coomassie staining of immunoprecipitates of oxidized KCNB1-HA channels run in reducing (20 mM DTT) or native (nondenaturing) conditions. The channels were oxidized with 2 mM H_2O_2 added for 10 min before lysis. The channels were expressed in HEK 293 cells because this cell type yields large amounts of protein that are needed for proper mass spectrometry analysis. ***C***, Western visualization (nondenaturing gel) of wild-type KCNB1-HA channels exposed to the indicated H_2O_2 amounts added for 5–10 min before lysis. In the last lane, samples oxidized with 5 mM H_2O_2 were run in reducing conditions (20 mM DTT). Inset, Densitometry quantification of the oligomer/monomer bands (oxidation ratio) following exposure to the indicated H_2O_2 concentrations. $n = 2–4$ experiments per point. ***D***, Western visualization (nondenaturing gel) of wild-type, C73A, and C73S KCNB1-HA channels transiently expressed in CHO cells in the absence or presence of 1.0 mM H_2O_2. The oxidant was added for 5–10 min before lysis. ***E***, As in ***C***, for C73A-KCNB1-HA channels. ***F***, Western visualization (nondenaturing gel) of the indicated KCNB1 variants exposed to 5 mM H_2O_2 for 5–10 min before lysis and run in native or reducing (20 mM DTT) conditions.

channels subsequently reduced with 20 mM DTT (Fig. 1*B*). The monomeric and oligomeric bands in the gel in Figure 1*B* were further analyzed by mass spectroscopy. This analysis confirmed that both bands contained only KCNB1 protein (Table 1). We conclude that the oligomers are the result of cross-linking of KCNB1 subunits to each other. Oxidative conditions in which a significant portion of the total KCNB1 protein existed in monomeric form, we define as mild. However, increasing the concentration of the oxidant such as in the experiment shown in Figure 1*C*, shifted the equilibrium toward the oligomeric states. We define the oxidation ratio, the densitometry ratio between the sum of the oligomeric bands and the monomeric band. This ratio increased from 0.38 ± 0.08 in 0.15 mM H_2O_2 to 1.7 ± 0.33 in 5 mM H_2O_2, a 4.5-fold increase. In those dose–response experiments we did not raise the concentration of H_2O_2 >5 mM to not cause extensive cellular damage. However, in agreement with the work of others (Zhang et al., 1996), high concentrations of H_2O_2 (25 mM) led to formation of high molecular weight aggregates which, in the absence of DTT, remained on the top of the stacking gel and did not migrate (data not shown). We conclude, that oxidative conditions induce KCNB1 oligomerization though modification of cysteine residues.

A conserved cysteine contributes to KCNB1 redox susceptibility

KVS-1, the *C. elegans* homolog of KCNB1, is susceptible to redox through a cysteine located in the N terminus (cys113) (Cai and Sesti, 2009) which is conserved in mammalian KCNB1 genes and corresponds to cys73 in the human channel. This sequence homology suggests that cys73 might play a role in determining KCNB1 susceptibility to redox. Therefore, we mutated cys73 to alanine (C73A) and to serine (C73S) which are considered the most conservative replacements for a cysteine. Both variants failed to oligomerize upon treatment with oxidants (Fig. 1*D*,*E*). However, while C73A gave rise to channels that were functionally indistinguishable from wild-type channels, C73S gave rise to nonconducting channels (see below). Therefore C73A was mostly used in this study. Nevertheless, the fact that KCNB1 exhibits multiple oligomeric species further implies that cys73 alone cannot mediate oligomerization—in this case the channel could only form dimers—and that at least another cysteine must be involved in the process. It has been shown that a subdomain in the N terminus containing cys73, physically interacts with the C terminus (Ju et al., 2003; Kobrinsky et al., 2006). This led us to speculate that the partner of cys73 might reside in the C terminus.

Table 1. Mass spectroscopy analysis

Peptide sequence	M_r Expected	M_r Experimental	Corresponding protein
Reduced			
SVLQFQNVR	1089.6397	1089.5931	gi|186798
FSHSPLTSLPSK	1299.7222	1299.6823	Voltage-gated potassium channel [*Homo sapiens*]gi 7331218
FSHSPLTSLPSK	1299.7496	1299.6823	
SIEMMDIVVEK	1324.6597	1324.6254	
NHFESSPLPTSPK	1439.7480	1439.7045	
LNVGGLAHEVLWR	1462.8349	1462.8045	
LNVGGLAHEVLWR	1462.8696	1462.8045	
QNCIYSTEALTGK	1483.7346	1483.6977	
GSAAAAVAGLECATLLDK	1716.9017	1716.8716	
GSAAAAVAGLECATLLDK	1716.9413	1716.8716	
SEKNHFESSPLPTSPK	1783.9530	1783.8741	
EELEMESIPSPVAPLPTR	2010.0274	2009.9979	
SMSSIDSFISCATDFPEATR	2236.9943	2236.9617	
FVEANPSPDASQHSSFFIESPK	2420.1906	2420.1284	
VNFMEGDPSPLLPVLGMYHDPLR	2628.3229	2628.2716	
ESAAQSKPKEELEMESIPSPVAPLPTR	2936.5740	2936.4800	
DCNTHDSLLEVCDDYSLDDNEYFFDR	3256.3466	3256.2874	
SLDLDSIIAEVK	1301.7429	1301.7078	gi|7331218
LNDLEDALQQAK	1356.7322	1356.6885	Keratin 1 [*Homo sapiens*]
SLNNQFASFIDK	1382.7232	1382.6830	
QISNLQQSISDAEQR	1715.8896	1715.8438	
Oxidized			
GSAAAAVAGLECATLLDK	1716.9171	1716.8716	gi|186798
SMSSIDSFISCATDFPEATR	2237.0033	2236.9617	Voltage-gated potassium channel [*Homo sapiens*]
SLDLDSIIAEVK	1301.7637	1301.7078	gi|119395750 Keratin, type II cytoskeletal 1 [*Homo sapiens*]

After tryptic digestion, protein fragments were ionized and detected by MS. The sequences of the detected fragments are listed in the first column. The predicted and observed molecular masses (M_r) of the fragments, expressed in Da, are given in the second and third columns, respectively. Mascot Server (Matrix Science) was used for database searching versus NCBInr (fourth column).

This domain contains three cysteine residues, namely cys594, cys710 and cys813. Therefore, we mutated them one by one to alanine and assessed the ability of the mutant channels to form oligomers. Following exposure to H_2O_2, the C594A and C813A mutants retained the ability to oligomerize, whereas the C710A variant formed only monomers (Fig. 1*F*). Similarly, the double C73A-C710A mutant did not oligomerize (Fig. 1*F*). Together, these data suggest that oxidative conditions lead to the formation of inter-subunit disulfide bridges between cys73 and cys710. This accounts for the presence of multiple oligomeric species in the gel and explains why mutation of a single cysteine of the pair is sufficient to disrupt oligomerization. Therefore, in the rest of this study we used the C73A mutant in our experiments.

Oxidants modify the KCNB1 current

To further elucidate the molecular basis for KCNB1 oxidation, also *in lieu* of the possible physiological implications of this modification, we transiently expressed the channel in mammalian (CHO) cells and electrophysiologically analyzed its currents. In control conditions, KCNB1 channels conducted robust, rapidly activating outward currents (Fig. 2*A*). Exposure to 1 mM CHT (Fig. 2*A*) or 1 mM H_2O_2 (data not shown) in the bath solution induced a marked decrease in the magnitude of the current density (Fig. 2*A*,*B*) along with a −11 mV shift in the half-maximal voltage for activation, $V_{1/2}$ ($V_{1/2} = 31.0 \pm 1.5$ mV in the absence and $V_{1/2} = 20.0 \pm 3.5$ mV in the presence of CHT, $n = 43$ cells, $p < 0.02$, Fig. 2*C*) and no appreciable changes in the V_s parameter ($V_s = 17.8 \pm 0.6$ mV in the absence and $V_s = 17.7 \pm 1.6$ mV in the presence of CHT, $n = 43$ cells). It must be noted that since prolonged exposure to oxidants cause cell damage, we primarily used CHT, which acted faster than H_2O_2 in electrophysiological assays. Macroscopic C73A currents were indistinguishable from wild-type current in magnitude and voltage dependence. In contrast, they were insensitive to both CHT (Fig. 2*A*,*B*) and H_2O_2 (data not shown). By contrast, the C73S variant expressed negligible amounts of current, which were also insensitive to CHT (Fig. 2*B*). To determine whether the macroscopic current decrease was caused by a reduction in the open probability, unitary conductance or both we performed single-channel analysis in inside-out patches. Representative recordings of the activity of single KCNB1 channels held at +80 mV in the absence/presence of 1 mM CHT are shown in Figure 2, *D* and *E*. Thus, KCNB1 was predominantly opened at +80 mV (Table 2). Brief exposure to 1 mM CHT in the bath markedly decreased the open probability of the channel from 0.6 to 0.07 without affecting its unitary current (1.1 pA vs 0.95 pA, Table 2). Wild-type channels retained normal activity upon patch excision in the absence of the oxidant (data not shown) ruling out the possibility that the rapid decline in channel's activity in the presence of CHT was due to run down. The properties of C73A channels did not differ from those of wild-type channels (Table 2). However, as expected, CHT had no noticeable effect on the activity of the channel (Fig. 2*E*). In whole-cell recordings, CHT decreased the open probability of the wild-type channel by ~70%, whereas in inside-out patches this effect was more marked (~ 93%). This could be caused by either incomplete diffusion of the oxidant into the cell, or alternatively by its partial inactivation by anti-oxidant defenses. We did not further investigate the causes for this discrepancy because an increase in either the time of exposure or concentration was often associated with considerable cellular damage.

KCNB1 oxidation contributes to neuronal apoptosis

To establish whether oxidation of KCNB1 is a mechanism of cytotoxicity, we assessed apoptosis in mammalian cells subject to oxidative insults transiently expressing wild-type, C73A or C73S KCNB1 channels. We performed these experiments in undifferentiated mouse neuroblastoma N2A cells and in CHO cells. The rationale for N2A cell is that they are neuronal cells and express endogenous KCNB1 channels (Leung et al., 2011) which carry most of the total N2A outward K^+ current (data not shown). This suggests that this channel is important for N2A cell function. To induce apoptosis, which was assessed by annexin-V staining, we used DTDP, because H_2O_2 is quickly detoxified by the glutathione system (Dringen, 2000). DTDP is a widely used apoptosis-inducing oxidant with high specificity for thiol groups (Brocklehurst, 1979). We biochemically confirmed that DTDP induced KCNB1 oligomerization (Fig. 3*A*). We initially monitored the levels of oxidative stress induced by DTDP treatment using the fluorimetric dye DCF, a generic ROS detector. Five minutes exposure to 10 μM DTDP immediately followed by removal of the oxidant, induced a rapid increase in DCF fluorescence which lasted for the entire course of the experiment (6 h, Fig. 3*B*,*C*). Thus, DTDP produced a long-lasting, stable condition of oxidative stress in the cell. Moreover, comparison of DCF intensity in DTDP- and H_2O_2-treated cells indicated that the oxidative stress induced by DTDP roughly corresponded to that of 0.3 mM H_2O_2 (36% increase in DCF fluorescence, data not shown), a concentration sufficient to induce KCNB1 oxidation. Accordingly, brief exposure of mock-transfected cells to DTDP in the 5–25 μM range induced significant apoptosis (Fig. 4*A*,*B*).

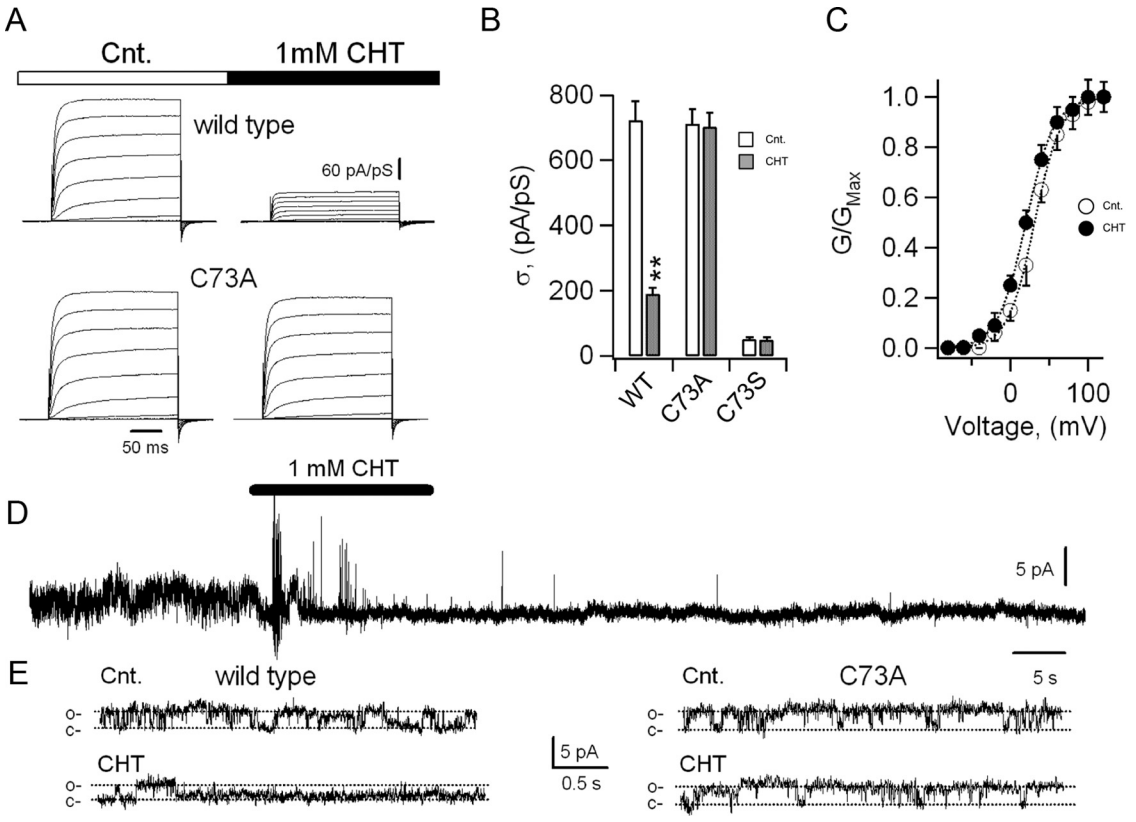

Figure 2. Oxidants modify the KCNB1 current. ***A***, Representative wild-type and C73A KCNB1 currents elicited by voltage jumps from −80 mV to +120 mV in 20 mV increments in the absence (control) and presence of 1.0 mM CHT for 5 min in the test solution. ***B***, Mean steady-state current density at +120 mV in control (hollow) and in the presence of CHT (light gray) for wild-type, C73A, and C73S. Data are from $n = 43$ (wild-type), $n = 18$ (C73A), and $n = 13$ (C73S) cells. ***C***, Normalized macroscopic conductance–*V* relationships (G/G_{Max}, Eq. 1) for wild-type KCNB1 channels in the absence (hollow circles) or presence (filled circles) of 1 mM CHT. $n = 43$. Fit to the Boltzmann function (dotted lines, Eq. 2) gave $V_{1/2} = 31.2$ mV and $V_s = 17.7$ mV in the absence and $V_{1/2} = 20.1$ mV and $V_s = 18.2$ mV in the presence of CHT. ***D***, Representative recording of a single KCNB1 channel in an inside-out patch in the absence/presence (indicated) of 1.0 mM CHT in the bath solution. ***E***, Activity of a single wild-type (left) or C73A (right) channel in the absence/presence of 1 mM CHT at an expanded time scale. Closed (c) and open (o) levels are indicated.

Table 2. Unitary properties of the KCNB1 channels at +80 mV

Control					1 mM CHT	
	i (pA)	p_o	τ_o (ms)	τ_c (ms)	*I* (pA)	p_o
WT ($n = 7$)	1.1 ± 0.4	0.58 ± 0.06	5.53 ± 0.81	14.7 ± 2.73	0.95 ± 0.4	0.07 ± 0.1
C73A ($n = 4$)	1.0 ± 0.4	0.67 ± 0.09	8.2 ± 1.10	14.3 ± 1.92	1.0 ± 0.3	0.72 ± 0.1

Inside-out patches were held at +80 mV during continuous recordings. Single-channel traces were acquired digitally and analyzed using the half-threshold method (Sakmann and Neher, 1995).

Cells expressing wild-type KCNB1 were more susceptible to apoptosis than mock-transfected cells in agreement with previous studies (Pal et al., 2003). Notably, cells expressing the C73A or C73S mutants exhibited a significantly lower rate of apoptotic death than cells transfected with wild type. By contrast, the number of cells undergoing necrosis, which does not depend on DTDP treatment, was significantly lower and most importantly remained fairly stable in all samples (staining with propidium iodide gave 5.9 ± 1.4, 8.4 ± 2.8, 6.0 ± 1.8 and 6.4 ± 2.2 per cent of necrotic cells in mock-, KCNB1-, C73A-, and C73S-transfected cells, respectively. DTDP = 25 μM). Similar results were obtained using CHO cells with the only difference that this cell line required higher concentrations of DTDP to induce apoptosis (50–100 μM, data not shown). The use of a marker such as annexin-V, which detects one of the earliest events in apoptosis—the externalization of phosphatidylserine—allowed us to assess the apoptotic process when cells were still alive (6 h postoxidation). To test the possibility that KCNB1 simply acted to accelerate the apoptotic process, we measured apoptosis 12 h postoxidation (Fig. 4*C*). Under these conditions, the number of cells positive to annexin-V was significantly larger in wild-type KCNB1 than mock- or C73A-transfected cells. Thus, KCNB1 truly acts to enhance apoptosis.

The finding that the nonconducting C73S mutant was cytoprotective (Fig. 4*B*), along with the observation that oxidation of KCNB1 resulted in a significant suppression of the current, indicated that the conducting properties of the channel were only partially responsible for its apoptotic effect, as previously proposed (Pal et al., 2003). On the other hand, protein aggregates, such as the oligomers formed by oxidized KCNB1, are well known to be toxic to cells through mechanisms not understood (for review, see Squier, 2001). Accordingly, DCF fluorescence was significantly increased in N2A cells expressing the wild-type channel compared with mock-transfected cells (Fig. 4*D*). Notably, in both C73A- and C73S-transfected cells, DCF fluorescence levels were comparable to control. Together, these results indicated that oxidation of KCNB1 can exacerbate apoptotic death in mammalian cells.

KCNB1 oxidation is exacerbated in mouse model of AD brain

The fact that KCNB1 is susceptible to redox might have profound implications for the function of the mammalian brain. Not only might it affect normal functions during senescence but in addition might become relevant to conditions such as Alzheimer's disease—KCNB1 is abundantly expressed in the pyramidal neurons of hippocampus and cortex (Misonou et al., 2005)—characterized by abnormal oxidative stress. To better understand the

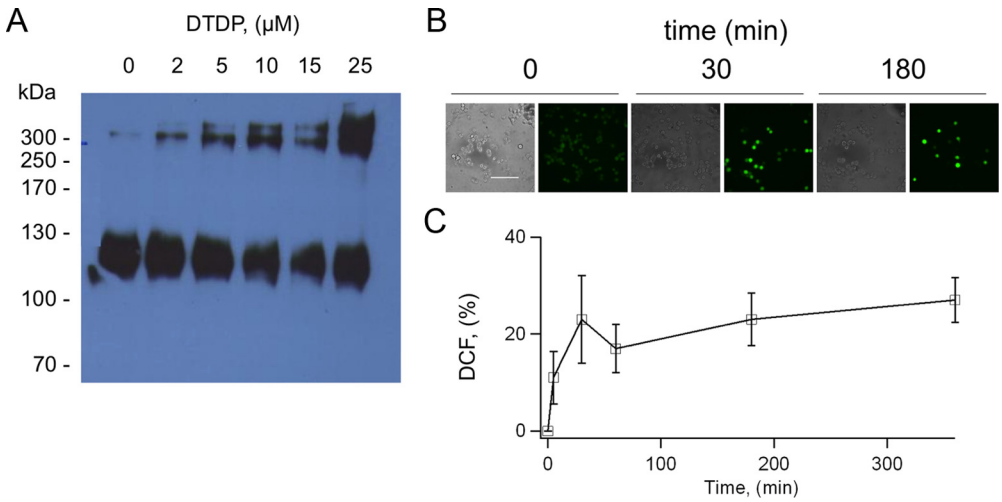

Figure 3. DTDP induces long-lasting oxidative stress in N2A cells. ***A***, Western visualization (nondenaturing gel) of wild-type KCNB1-HA channels transiently expressed in N2A cells and oxidized with the indicated amounts of DTDP for 5–10 min before lysis. ***B***, Representative images (bright light and DCF-fluorescence) of mock-transfected N2A cells exposed to 10 μM DTDP at the indicated time points. Scale bar, 10 μm. ***C***, Time course of DCF-fluorescence in N2A cells exposed to 10 μM DTDP. Data are expressed as percentage increase in fluorescence with respect to control cells. $n = 4$ experiments.

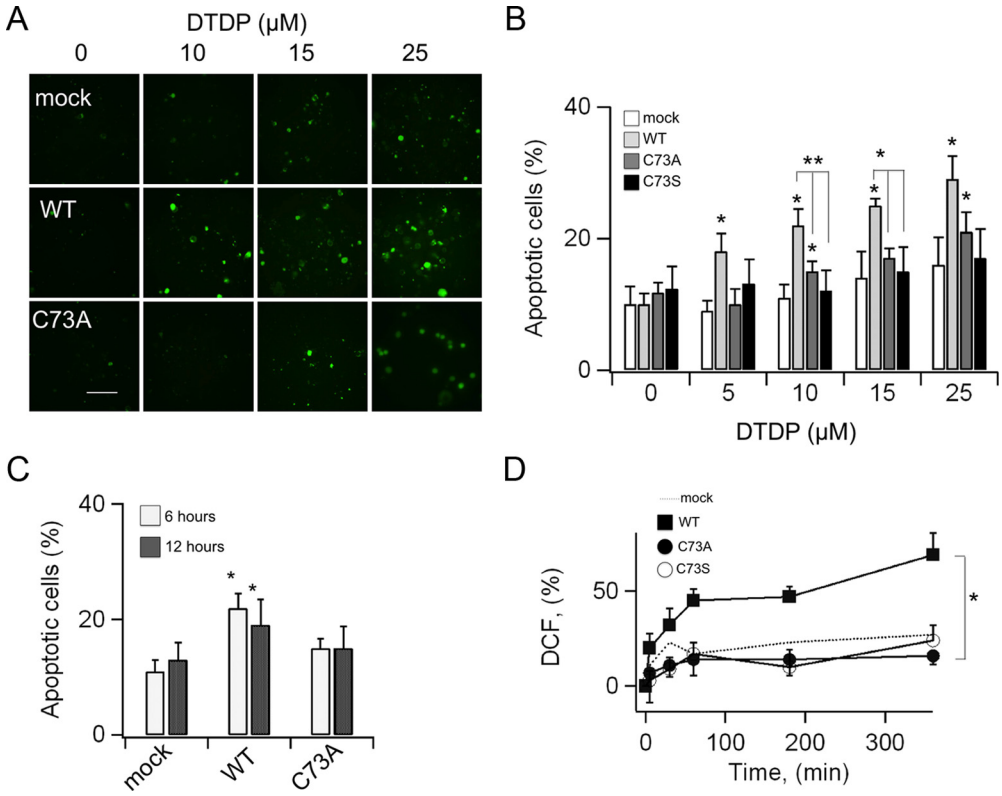

Figure 4. C73A protects N2A cells from oxidative stress. ***A***, Representative images of N2A cells stained with annexin-V. Cells were transfected with the indicated cDNA constructs and exposed at the indicated concentrations of DTDP. Scale bar, 10 μm. ***B***, Number of cells positive to annexin-V in mock (hollow)-, wild-type KCNB1 (light gray)-, C73A (dark gray)-, and C73S (black)-transfected cells following exposure to the indicated concentrations of DTDP. Cells were measured 6 h postoxidation. $n = 3$–9 experiments. ***C***, Number of cells positive to annexin-V 6 (hollow) and 12 (dark gray) h postoxidation. DTDP = 10 μM. $n = 6$ and 4 experiments, respectively. ***D***, Time course of DCF-fluorescence in N2A cells transfected with wild-type (squares), C73A (filled circles), and C73S (hollow circles), following exposure to 10 μM DTDP. Dotted line, Mock-transfected cells. $n = 4$, 5, and 3 experiments for, respectively, wild-type, C73A, and C73S. Statistical confidence is indicated as $^*p < 0.05$. Symbols on top of the error bar indicate a statistical confidence (calculated by a *t* test) between the indicated data and the corresponding control.

physiological role of KCNB1 oxidation we biochemically characterized KCNB1 channels in the brain of normal (wild-type) and mouse models of AD of either sex. Toward this end we used the 3xTg-AD transgenic mouse which provides one of the most comprehensive mice models of AD by harboring PS1(M146V), APP_{Swe}, and tau_{P301L} transgenes (Oddo et al., 2003). Moreover, oxidative stress is extensive in the brain of the 3xTg-AD mouse (Smith et al., 2005; Sensi et al., 2008; Yao et al., 2009; Chou et al., 2011; McManus et al., 2011). The Western blot in Figure 5*A*, shows KCNB1 protein levels in brains of 2-, 11-, and 22-month-old animals blotted under reducing conditions (20 mM DTT). In both wild-type and 3xTg-AD brain, KCNB1 exhibited a marked

downregulation between 2 and 11 months (Fig. 5*B*). In older animals (22 months), KCNB1 protein levels were higher in wild-type than AD brains most likely due to the significant neuronal loss occurring in the latter at this age (Oddo et al., 2003). However, KCNB1 downregulation was not AD-dependent and rather appeared to be a normal phenomenon in mice aging brain. Therefore we did not investigate this phenomenon further. Native Western blots of KCNB1 channels from wild-type and 3xTg-AD brains are shown in Figure 5*C*. In 2-month-old brains, KCNB1 channels run as monomers in both wild-type and AD mice. In older animals however, KCNB1 showed typical signs of oxidation. That is, oligomeric bands running with molecular masses ranging from ~ 250 kDa to ~400 kDa which were abolished by DTT. Most importantly, these bands were significantly more abundant in 3xTg-AD than wild type (Fig. 5*D*). The oligomerization patterns in mice brains and heterologous expression systems were similar but not identical. This was probably due to intrinsic differences of the systems. Together, these data suggest that like in invertebrates, K^+ channels are subject to a natural process of oxidation during aging and most importantly, that this oxidation is exacerbated in AD brain.

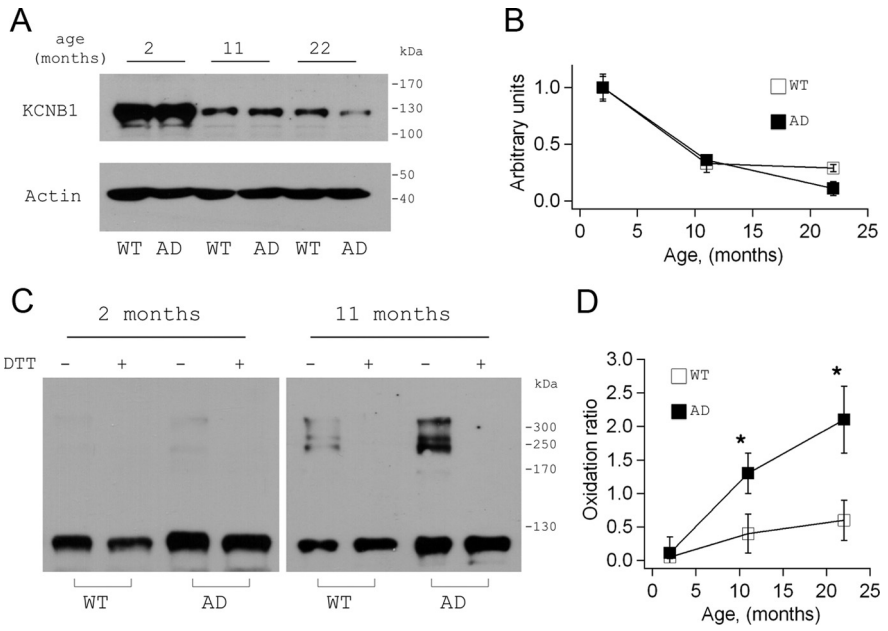

Figure 5. Native KCNB1 channels are oxidized in 3xTg-AD mouse brain. ***A***, Representative Western visualization of KCNB1 channels in brains of control and 3xTg-AD mouse at the indicated ages. KCNB1 channels were detected using a polyclonal antibody from Millipore. ***B***, Densitometry quantification of the amount of KCNB1 protein detected in homogenized brains of control (WT, hollow) or 3xTg-AD (AD, filled) mice at the indicated time points. $n = 5–6$ samples per point. ***C***, Representative Western blot visualization of KCNB1 channels in the brains of control and 3xTg-AD mice in the absence of denaturing agents (native) and the absence/presence of 20 mM DTT. In these experiments samples were loaded to have roughly the same amount of monomer. Therefore, these gels do not necessarily indicate the absolute amount of protein. ***D***, KCNB1 oxidation ratio in control (WT, hollow) and 3xTg-AD (AD, filled) brains. $n = 5–6$ samples per point.

β-amyloid induces KCNB1 oxidation

Aβ oligomers contribute to increasing oxidative stress in AD neurons through multiple mechanisms and pathways (Hensley et al., 1994; Canevari et al., 1999; Lustbader et al., 2004; Takuma et al., 2005; Crouch et al., 2006; Manczak et al., 2006; Shelat et al., 2008; Rhein et al., 2009; Saraiva et al., 2010). It follows that Aβ might indirectly induce oxidation of KCNB1 channels in AD brain. We initially tested this hypothesis in N2A cells. Thus, when the cells were exposed to recombinant, solubilized, $A\beta_{1-42}$ peptide (23 μM, a concentration which did not induce significant toxicity in control cells over the period of the experiment, 12 h) DCF fluorescence which gave a measure of oxidative stress in our assays, increased by 27% compared with untreated cells (Fig. 6*A*), an increase comparable to that induced by 10 μM DTDP. Accordingly, $A\beta_{1-42}$, was associated with the formation of channel's oligomers in a time-dependent fashion (Fig. 6*B*). Apoptosis increased by ~30% in mock-transfected cells incubated with the peptide (Fig. 6*C*). Apoptosis was significantly enhanced, by ~100%, in cells expressing wild-type KCNB1. By contrast, transfection with the C73A mutant reduced apoptosis to control values. Control tests, performed using the reverse peptide $A\beta_{42-1}$, did not reveal any increase in apoptosis (Fig. 6*D*). Together, these data suggested that in N2A cells, $A\beta_{1-42}$-induced oxidation of KCNB1 channels constituted a mechanism of cytotoxicity.

Oxidation of K^+ channels is neurotoxic in a *C. elegans* model of AD

To further explore the notion that oxidation of K^+ channels is a contributing factor to neurotoxicity in AD, we tested this mechanism in animal systems. To this end we used the nematode *C. elegans* to construct a model that mimics aspects of the disease. Thus, we engineered transgenic worms expressing human $A\beta_{1-42}$ protein in the ASE sensory neurons (Fig. 7*A*), which are crucially dependent on a KCNB1 homolog, the KVS-1 channel (Bianchi et al., 2003). The strains expressing $A\beta_{1-42}$ were normally viable, presumably because the expression of the peptide was circumscribed to a few, well characterized neurons. As such, the function of other organs and cells was not affected. In particular locomotion, which is crucially dependent on KVS-1 (Bianchi et al., 2003) was normal in these strains (99.5 ± 3; 102.5 ± 2; 102.3 ± 3 and 100.2 ± 4 thrashes/min for N2 ($n = 9$), N2 +$A\beta_{1-42}$ ($n = 8$), WT+$A\beta_{1-42}$ ($n = 10$) and N2 +$A\beta_{1-42}$ ($n = 10$) respectively). Accordingly, chemotaxis to biotin, a gustatory function specifically mediated by the ASE neurons, was significantly compromised after the first week of life in parental worms expressing $A\beta_{1-42}$ and in transgenic worms expressing wild-type KVS-1 and $A\beta_{1-42}$ in a *kvs-1* KO background (Fig. 6*B*). Notably, the loss of chemosensory function was markedly reduced in worms expressing the oxidation-resistant C113S-KVS-1 variant. It must be noted that an important feature of the *C. elegans* system is the fact that the *kvs-1* KO current is not susceptible to redox and that transgenic rescue of KVS-1 and C113S does not lead to overexpression (Cai and Sesti, 2009). As such, this worm provided an important, direct test of causality not easily undertaken in other model systems. Consistent with behavioral results, ~50% of cultured ASE neurons died within the first 10 d of life, whereas neurons expressing C113S-KVS-1 survived at a much higher rate (Fig. 7*C*). To gain insight into the mechanism of death, we grew the worms in the presence of a caspase inhibitor, *N*-(2-quinolyl)valyl-aspartyl-(2,6-difluorophenoxy)methyl ketone (Q-VD-OPh), which has demonstrated broad-spectrum efficacy in affording neuroprotection in animal models of AD (Caserta et al., 2003). The rationale

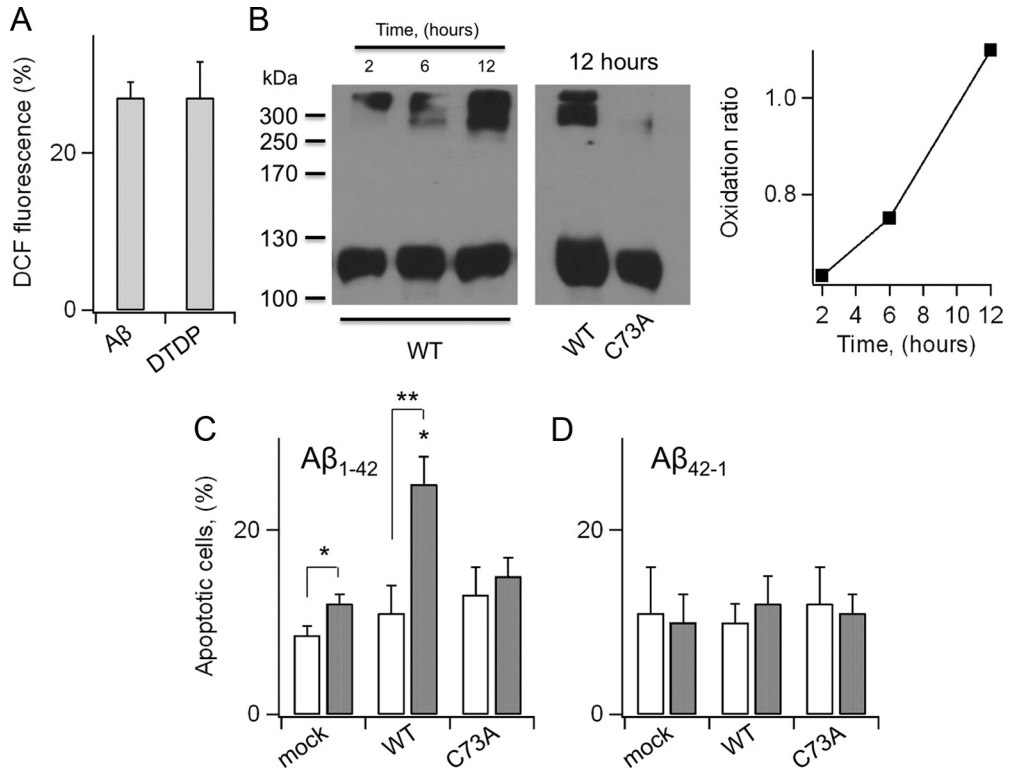

Figure 6. C73A protects N2A from $A\beta_{1-42}$. ***A***, DCF-fluorescence in N2A cells grown in the presence of 23 μg/ml solubilized $A\beta_{1-42}$ in the media for 12 h. For comparison, DCF fluorescence in cells treated for 5 min with 10 μM DTDP. Data are expressed as percentage increases in DCF fluorescence with respect to control cells. $n = 3$ experiments. ***B***, Western visualization (nondenaturing gel) of wild-type (left gel) and C73A (right gel) KCNB1-HA channels incubated with 23 μM recombinant $A\beta_{1-42}$ at the indicated time points. Inset, Oxidation ratio of the experiment shown in the left gel. ***C***, Number of cells positive to annexin-V in mock-, wild-type KCNB1-, and C73A-transfected cells grown in the absence (hollow) or presence (gray) of 23 μg/ml solubilized, not aggregatable $A\beta_{1-42}$ peptide. $n = 4–7$ experiments. ***D***, Number of cells positive to annexin-V in mock-, wild-type KCNB1-, and C73A-transfected cells grown in the absence (hollow) or presence (gray) of 23 μg/ml reverse $A\beta_{42-1}$ peptide. $n = 3$ experiments.

for this pharmacological approach was twofold: first, activation of caspases and cleavage of critical cellular proteins is crucially associated with apoptotic death (Rohn and Head, 2008, 2009), and second, it afforded the possibility to carry out quantitative analysis in living animals. Treatment with Q-VD-OPh completely and selectively stopped the loss of chemosensory function in worms expressing $A\beta_{1-42}$ (Fig. 7*D*), consistent with the notion that these cells undergo apoptosis. In summary, lack of oxidative modification in K^+ channels confers protection in *C. elegans* neurons expressing $A\beta_{1-42}$. This shows, for the first time, that in a living organism there is a link between the increase in oxidative stress associated with the presence of $A\beta_{1-42}$ in the cell and the K^+ current.

Discussion

To elucidate fundamental questions about the role that oxidation of K^+ channels has for the function of the mammalian brain, we studied neuronal voltage-gated KCNB1 channels expressed *in vitro* (mammalian cells) and *in vivo* (mouse brain). We found that KCNB1 is a redox-susceptible channel. Oxidative conditions induce channel's oligomerization through the formation of intersubunit disulfide bridges which give rise to nonactivating channels. KCNB1 proteins are oxidized in aging mouse brain and most importantly their oxidation is exacerbated in AD. In both mammalian cell lines and in a *C. elegans* model that mimics aspects of AD, mutant channels that are insensitive to oxidation, prolong neuronal survival in a variety of oxidative challenges. Thus, oxidation of K^+ channels appears to be a general mechanism of neurotoxicity in living organisms.

The redox properties of rat KCNB1 channels were previously investigated by Zhang and colleagues in an attempt to probe interacting domains in the pore of the protein (Zhang et al., 1996). The high concentration of H_2O_2 (0.1% equivalent to ~30 mM) used in that study, led to the formation of insoluble, high molecular weight aggregates—consequence of massive cross-linking between subunits—leading the investigators to conclude that KCNB1 cannot be oxidated. Our results show that on the contrary, KCNB1 is exquisitely susceptible to redox. As such, channel's oxidation proceeds in a dose-dependent fashion, giving rise to specific oligomeric species consistent with dimer, trimer and tetramer formation when the concentration of H_2O_2 is low and ending, as H_2O_2 levels are raised, in the formation of unspecific aggregates which cannot migrate in the gel when DTT is absent. There is consensus around a model that predicts that a domain in the N terminus containing cys73 and the C terminus activation (CTA) domain, which is flanked by cys710, physically interact during channel's activation (Ju et al., 2003; Kobrinsky et al., 2006). The observation that cys73–cys710 form disulfide bridges corroborates the existing knowledge of the channel and may explain why its oxidation decreases the open probability: by presumably locking the protein in a configuration which prevents further structural rearrangements that are necessary for activation. The crucial role of cys73 for KCNB1 function is further underscored by the observation that replacement of this residue with a serine is sufficient to give rise to nonfunctional channels. This may have evolutionary relevance and may explain why Cys is conserved in KCNB1 channels of different species even

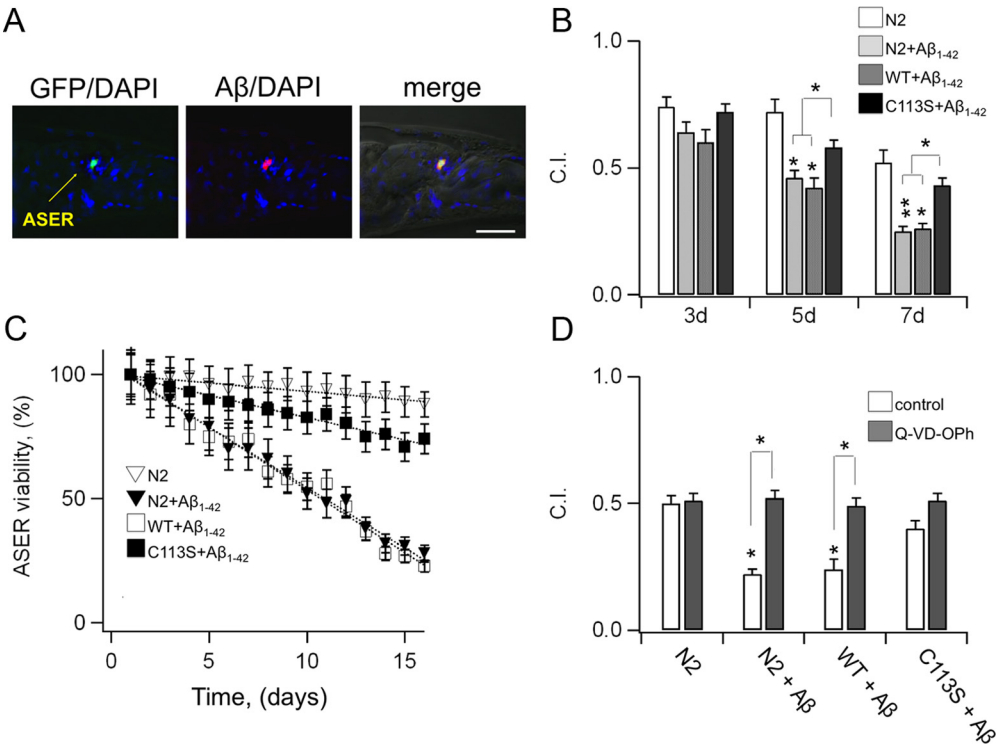

Figure 7. In a *C. elegans* model of AD, a K^+ channel resistant to oxidative stress protects the neurons from apoptotic death. ***A***, Anterior region of transgenic worm (strain FDX(*ses25*)) expressing P*gcy-5*::GFP and P*flp-6*::Aβ_{1-42} constructs, probed with anti-Aβ_{1-42} monoclonal antibody 6E10 and DNA stain DAPI. Shown is a single optical section (1 μm) from a deconvolution series. Left, GFP (green) + DAPI (blue) signal; middle, Aβ (red) + DAPI; right, fused epifluorescence images overlain on DIC image. Scale bar, 20 μm. ***B***, Chemotaxis to biotin in parental worms (N2, hollow) and in transgenic worms expressing human Aβ_{1-42} in the ASE neurons of N2 (FDX(*ses19*), light gray), wild-type KVS-1 (FDX(*ses21*), dark gray), and C113S-KVS-1 (FDX(*ses20*), black), at the indicated time points. $n = 4$ experiments. ***C***, Viability of cultured, age-synchronized, ASE right (ASER) neurons in N2 worms (hollow triangles) and in transgenic worms expressing human Aβ_{1-42} in the ASE neurons of N2 (FDX(*ses25*), filled triangles), wild-type KVS-1 (FDX(*ses27*), hollow squares), and C113S-KVS-1 (FDX(*ses26*), filled squares), at the indicated time points. The ASER neurons were marked with the *gcy-5*::GFP reporter, which drives GFP expression only in the ASER neuron. The disappearance of GFP fluorescence was used as a measure of a neuron's viability. A single experiment started with 300–500 fluorescent cells. Data were calculated as 100*(number of fluorescent cells at day *X* divided by number of fluorescent cells at day 1). $n = 3$ experiments. ***D***, Chemotaxis to biotin in 9-d-old N2 worms and in transgenic worms expressing human Aβ_{1-42} in the ASE neurons of N2 (FDX(*ses19*)), wild-type KVS-1 (FDX(*ses21*)), and C113S-KVS-1 (FDX(*ses20*)) grown in the absence (hollow) or presence (gray) of 1 μg/ml Q-VD-OPh. Worms were maintained at 20°C in liquid cultures (S medium). Q-VD-OPh was administered daily. Prior to the experiment, worms were placed in ice for 15 min to settle, the medium was gently aspirated, and then they were washed in M9 buffer and collected in 50 ml Falcon tubes. The difference between the strains used in these experiments and in behavioral assays resides in the different markers used for the transformation (see Materials and Methods).

though its oxidation alters channel's function. A meticulous biophysical analysis will elucidate the details of these mechanisms in the near future.

Oxidative stress occurs early in AD, before the beginning of significant plaque formation. The fact that KCNB1 channels are over-oxidized in 3xTg-AD brain implies that oxidation of this protein may contribute to neurotoxicity in early disease stages. By hampering neuronal excitability, prematurely oxidized KCNB1 channels might confer disease susceptibility well before the onset of significant neuronal loss. Moreover, in both mammalian cells and animal models (*C. elegans*) redox-insensitive K^+ channel variants were protective against apoptosis, suggesting that a condition of chronic oxidation of these channels might contribute to trigger apoptotic responses in neurons. The KCNB1 channel has been dubbed proapoptotic because an increase in K^+ efflux mediated by this protein constitutes an important step during neuronal apoptosis (Pal et al., 2003). Studies have shown that during oxidant-induced apoptosis, release of Zn^{2+} from metalloproteins (mediated by DTDP; Aizenman et al., 2000), leads to the insertion of newly synthesized KCNB1 channels into the plasma membrane through a pathway that requires p38 MAPK phosphorylation of KCNB1 at ser800 (Redman et al., 2007). Our findings corroborate the notion that KCNB1 is a proapoptotic protein, because its expression exacerbated apoptosis in mammalian cells subject to oxidative insults. However, they are not consistent with the present model that predicts that a surge in the channel's current—which is drastically reduced in oxidized channels—is sufficient, alone, to trigger apoptosis (Pal et al., 2003). Our observations suggest that the formation of KCNB1 oligomers and the consequent increase in oxidative stress, are the underlying causes for its toxicity. Even though a detailed elucidation of the mechanism through which oxidation of KCNB1 leads to apoptosis goes beyond the scope of this study and will be the matter of a future investigation we speculate that the formation of disulfide bridges linking the N and C termini might give rise to channels resistant to proteolytic cleavage or hamper their internalization/endocytosis. These mechanisms would be consistent with increased KCNB1 surface expression, for example as a result of impaired retrograde transport, without implying a corresponding increase in the current. Thus, the observation that KCNB1 forms oligomers, provides another example of ROS-induced "aggregating protein toxicity" typical of neurodegenerative diseases such as AD, which are characterized by high levels of oxidative stress (Squier, 2001). Moreover, the time at which changes in the KCNB1 current begin to occur might be critical. Evidence shows that in cerebellar granule neurons, increases in ROS levels and changes in K^+ currents must be timely synchronized to induce apoptosis (Hernández-Enríquez et al., 2011).

Specifically, only early surges in K^+ effluxes are proapoptotic. Referred to KCNB1, this might be relevant to *in vivo* conditions where oxidation of the channel is likely to proceed more gradually than in *in vitro* systems. Future studies will elucidate the mechanism through which oxidation of KCNB1 causes toxicity in detail. Nevertheless, an important concept emerges from this study: that preservation of normal KCNB1 function, such as in the C73A variant, represents an effective mechanism of neuroprotection against oxidation-induced apoptosis.

The observation that KCNB1 can be oxidated prompts implications that go beyond the role of this channel in the brain. An example in this sense is provided by the closure of the human ductus arteriosus within minutes of birth. As changes in oxygen levels are sensed by the mitochondrial electron transport chain, it responds by increasing the amounts of diffusible H_2O_2. This, in turn, activates a not well defined oxygen sensor, which is postulated to mediate the inhibition of voltage-gated K^+ channels, including KCNB1—that control vascular tone, causing vasoconstriction (Michelakis et al., 2002). Thus, the finding that the KCNB1 channel can directly respond to H_2O_2, challenges the need for an oxygen sensor and may stimulate further investigation in this direction.

References

Aizenman E, Stout AK, Hartnett KA, Dineley KE, McLaughlin B, Reynolds IJ (2000) Induction of neuronal apoptosis by thiol oxidation: putative role of intracellular zinc release. J Neurochem 75:1878–1888.

Bianchi L, Kwok SM, Driscoll M, Sesti F (2003) A potassium channel-MiRP complex controls neurosensory function in *Caenorhabditis elegans*. J Biol Chem 278:12415–12424.

Brocklehurst K (1979) Specific covalent modification of thiols: applications in the study of enzymes and other biomolecules. Int J Biochem 10:259–274.

Butterfield DA, Lauderback CM (2002) Lipid peroxidation and protein oxidation in Alzheimer's disease brain: potential causes and consequences involving amyloid beta-peptide-associated free radical oxidative stress. Free Radic Biol Med 32:1050–1060.

Cai SQ, Sesti F (2009) Oxidation of a potassium channel causes progressive sensory function loss during aging. Nat Neurosci 12:611–617.

Canevari L, Clark JB, Bates TE (1999) beta-Amyloid fragment 25–35 selectively decreases complex IV activity in isolated mitochondria. FEBS Lett 457:131–134.

Caserta TM, Smith AN, Gultice AD, Reedy MA, Brown TL (2003) Q-VD-OPh, a broad spectrum caspase inhibitor with potent antiapoptotic properties. Apoptosis 8:345–352.

Chou JL, Shenoy DV, Thomas N, Choudhary PK, Laferla FM, Goodman SR, Breen GA (2011) Early dysregulation of the mitochondrial proteome in a mouse model of Alzheimer's disease. J Proteomics 74:466–479.

Crouch PJ, Barnham KJ, Duce JA, Blake RE, Masters CL, Trounce IA (2006) Copper-dependent inhibition of cytochrome *c* oxidase by Abeta(1–42) requires reduced methionine at residue 35 of the Abeta peptide. J Neurochem 99:226–236.

Dringen R (2000) Metabolism and functions of glutathione in brain. Prog Neurobiol 62:649–671.

Harman D (1956) Aging: a theory based on free radical and radiation chemistry. J Gerontol 11:298–300.

Hensley K, Carney JM, Mattson MP, Aksenova M, Harris M, Wu JF, Floyd RA, Butterfield DA (1994) A model for beta-amyloid aggregation and neurotoxicity based on free radical generation by the peptide: relevance to Alzheimer disease. Proc Natl Acad Sci U S A 91:3270–3274.

Hensley K, Hall N, Subramaniam R, Cole P, Harris M, Aksenov M, Aksenova M, Gabbita SP, Wu JF, Carney JM, et al. (1995) Brain regional correspondence between Alzheimer's disease histopathology and biomarkers of protein oxidation. J Neurochem 65:2146–2156.

Hernández-Enríquez B, Guemez-Gamboa A, Morán J (2011) Reactive oxygen species are related to ionic fluxes and volume decrease in apoptotic cerebellar granule neurons: role of NOX enzymes. J Neurochem 117:654–664.

Ju M, Stevens L, Leadbitter E, Wray D (2003) The Roles of N- and C-terminal determinants in the activation of the Kv2.1 potassium channel. J Biol Chem 278:12769–12778.

Kobrinsky E, Stevens L, Kazmi Y, Wray D, Soldatov NM (2006) Molecular rearrangements of the Kv2.1 potassium channel termini associated with voltage gating. J Biol Chem 281:19233–19240.

Kullmann DM (2002) The neuronal channelopathies. Brain 125:1177–1195.

Lauderback CM, Hackett JM, Huang FF, Keller JN, Szweda LI, Markesbery WR, Butterfield DA (2001) The glial glutamate transporter, GLT-1, is oxidatively modified by 4-hydroxy-2-nonenal in the Alzheimer's disease brain: the role of Abeta1–42. J Neurochem 78:413–416.

Leung YM, Huang CF, Chao CC, Lu DY, Kuo CS, Cheng TH, Chang LY, Chou CH (2011) Voltage-gated K(+) channels play a role in cAMP-stimulated neuritogenesis in mouse neuroblastoma N2A cells. J Cell Physiol 226:1090–1098.

Lin MT, Beal MF (2006) Mitochondrial dysfunction and oxidative stress in neurodegenerative diseases. Nature 443:787–795.

Link CD (1995) Expression of human beta-amyloid peptide in transgenic *Caenorhabditis elegans*. Proc Natl Acad Sci U S A 92:9368–9372.

Link CD, Silverman MA, Breen M, Watt KE, Dames SA (1992) Characterization of *Caenorhabditis elegans* lectin-binding mutants. Genetics 131:867–881.

Lustbader JW, Cirilli M, Lin C, Xu HW, Takuma K, Wang N, Caspersen C, Chen X, Pollak S, Chaney M, Trinchese F, Liu S, Gunn-Moore F, Lue LF, Walker DG, Kuppusamy P, Zewier ZL, Arancio O, Stern D, Yan SS, et al. (2004) ABAD directly links Abeta to mitochondrial toxicity in Alzheimer's disease. Science 304:448–452.

Manczak M, Anekonda TS, Henson E, Park BS, Quinn J, Reddy PH (2006) Mitochondria are a direct site of A beta accumulation in Alzheimer's disease neurons: implications for free radical generation and oxidative damage in disease progression. Hum Mol Genet 15:1437–1449.

Mankouri J, Dallas ML, Hughes ME, Griffin SD, Macdonald A, Peers C, Harris M (2009) Suppression of a pro-apoptotic K+ channel as a mechanism for hepatitis C virus persistence. Proc Natl Acad Sci U S A 106:15903–15908.

McManus MJ, Murphy MP, Franklin JL (2011) The mitochondria-targeted antioxidant MitoQ prevents loss of spatial memory retention and early neuropathology in a transgenic mouse model of Alzheimer's disease. J Neurosci 31:15703–15715.

Michelakis ED, Rebeyka I, Wu X, Nsair A, Thébaud B, Hashimoto K, Dyck JR, Haromy A, Harry G, Barr A, Archer SL (2002) O2 sensing in the human ductus arteriosus: regulation of voltage-gated K^+ channels in smooth muscle cells by a mitochondrial redox sensor. Circ Res 91:478–486.

Misonou H, Mohapatra DP, Trimmer JS (2005) Kv2.1: a voltage-gated K^+ channel critical to dynamic control of neuronal excitability. Neurotoxicology 26:743–752.

Nunomura A, Perry G, Aliev G, Hirai K, Takeda A, Balraj EK, Jones PK, Ghanbari H, Wataya T, Shimohama S, Chiba S, Atwood CS, Petersen RB, Smith MA (2001) Oxidative damage is the earliest event in Alzheimer disease. J Neuropathol Exp Neurol 60:759–767.

Oddo S, Caccamo A, Shepherd JD, Murphy MP, Golde TE, Kayed R, Metherate R, Mattson MP, Akbari Y, LaFerla FM (2003) Triple-transgenic model of Alzheimer's disease with plaques and tangles: intracellular Abeta and synaptic dysfunction. Neuron 39:409–421.

Pal S, Hartnett KA, Nerbonne JM, Levitan ES, Aizenman E (2003) Mediation of neuronal apoptosis by Kv2.1-encoded potassium channels. J Neurosci 23:4798–4802.

Park KH, Hernandez L, Cai SQ, Wang Y, Sesti F (2005) A family of K^+ channel ancillary subunits regulate taste sensitivity in *Caenorhabditis elegans*. J Biol Chem 280:21893–21899.

Praticò D, Uryu K, Leight S, Trojanoswki JQ, Lee VM (2001) Increased lipid peroxidation precedes amyloid plaque formation in an animal model of Alzheimer amyloidosis. J Neurosci 21:4183–4187.

Reddy PH, McWeeney S, Park BS, Manczak M, Gutala RV, Partovi D, Jung Y, Yau V, Searles R, Mori M, Quinn J (2004) Gene expression profiles of transcripts in amyloid precursor protein transgenic mice: up-regulation of mitochondrial metabolism and apoptotic genes is an early cellular change in Alzheimer's disease. Hum Mol Genet 13:1225–1240.

Redman PT, He K, Hartnett KA, Jefferson BS, Hu L, Rosenberg PA, Levitan ES, Aizenman E (2007) Apoptotic surge of potassium currents is mediated by p38 phosphorylation of Kv2.1. Proc Natl Acad Sci U S A 104:3568–3573.

Rhein V, Song X, Wiesner A, Ittner LM, Baysang G, Meier F, Ozmen L,

Bluethmann H, Dröse S, Brandt U, Savaskan E, Czech C, Götz J, Eckert A (2009) Amyloid-beta and tau synergistically impair the oxidative phosphorylation system in triple transgenic Alzheimer's disease mice. Proc Natl Acad Sci U S A 106:20057–20062.

Rohn TT, Head E (2008) Caspase activation in Alzheimer's disease: early to rise and late to bed. Rev Neurosci 19:383–393.

Rohn TT, Head E (2009) Caspases as therapeutic targets in Alzheimer's disease: is it time to "cut" to the chase? Int J Clin Exp Pathol 2:108–118.

Rojas P, Garst-Orozco J, Baban B, de Santiago-Castillo JA, Covarrubias M, Salkoff L (2008) Cumulative activation of voltage-dependent KVS-1 potassium channels. J Neurosci 28:757–765.

Sakmann B, Neher E, eds (1995) Single-channel recording, Ed 2. New York: Plenum.

Saraiva LM, Seixas da Silva GS, Galina A, da-Silva WS, Klein WL, Ferreira ST, De Felice FG (2010) Amyloid-beta triggers the release of neuronal hexokinase 1 from mitochondria. PLoS One 5:e15230.

Sensi SL, Rapposelli IG, Frazzini V, Mascetra N (2008) Altered oxidant-mediated intraneuronal zinc mobilization in a triple transgenic mouse model of Alzheimer's disease. Exp Gerontol 43:488–492.

Sesti F, Liu S, Cai SQ (2010) Oxidation of potassium channels by ROS: a general mechanism of aging and neurodegeneration? Trends Cell Biol 20:45–51.

Shelat PB, Chalimoniuk M, Wang JH, Strosznajder JB, Lee JC, Sun AY, Simonyi A, Sun GY (2008) Amyloid beta peptide and NMDA induce ROS from NADPH oxidase and AA release from cytosolic phospholipase A2 in cortical neurons. J Neurochem 106:45–55.

Smith IF, Hitt B, Green KN, Oddo S, LaFerla FM (2005) Enhanced caffeine-induced Ca^{2+} release in the 3xTg-AD mouse model of Alzheimer's disease. J Neurochem 94:1711–1718.

Song WJ (2002) Genes responsible for native depolarization-activated K^+ currents in neurons. Neurosci Res 42:7–14.

Squier TC (2001) Oxidative stress and protein aggregation during biological aging. Exp Gerontol 36:1539–1550.

Sultana R, Perluigi M, Butterfield DA (2006) Protein oxidation and lipid peroxidation in brain of subjects with Alzheimer's disease: insights into mechanism of neurodegeneration from redox proteomics. Antioxid Redox Signal 8:2021–2037.

Takuma K, Yao J, Huang J, Xu H, Chen X, Luddy J, Trillat AC, Stern DM, Arancio O, Yan SS (2005) ABAD enhances Abeta-induced cell stress via mitochondrial dysfunction. FASEB J 19:597–598.

Vernino S (2007) Autoimmune and paraneoplastic channelopathies. Neurotherapeutics 4:305–314.

Yao J, Irwin RW, Zhao L, Nilsen J, Hamilton RT, Brinton RD (2009) Mitochondrial bioenergetic deficit precedes Alzheimer's pathology in female mouse model of Alzheimer's disease. Proc Natl Acad Sci U S A 106:14670–14675.

Zhang HJ, Liu Y, Zühlke RD, Joho RH (1996) Oxidation of an engineered pore cysteine locks a voltage-gated K^+ channel in a nonconducting state. Biophys J 71:3083–3090.